ELSEVIER

Contents lists available at ScienceDirect

BBA - Molecular Basis of Disease

journal homepage: www.elsevier.com/locate/bbadis





NMN recruits GSH to enhance GPX4-mediated ferroptosis defense in UV irradiation induced skin injury

Zhuan Feng ^{a,1}, Yifei Qin ^{b,1}, Fei Huo ^{a,1}, Zhe Jian ^c, Xiaomin Li ^a, Jiejie Geng ^{a,*}, Yong Li ^{a,d,*}, Jiao Wu ^{a,*}

- a National Translational Science Center for Molecular Medicine & Department of Cell Biology, Fourth Military Medical University, Xi'an 710032, China
- ^b School of Pharmacy, Guangdong Pharmaceutical University, Guangzhou 510000, China
- ^c Department of Dermatology, Xijing Hospital, Fourth Military Medical University, Xi'an 710032, China
- ^d The Second Affiliated Hospital of Xi'an Jiaotong University, Xi'an 710004, China

ARTICLEINFO

Keywords: Skin injury Ferroptosis NMN

ABSTRACT

Oxidative stress and lipid peroxidation are major causes of skin injury induced by ultraviolet (UV) irradiation. Ferroptosis is a form of regulated necrosis driven by iron-dependent peroxidation of phospholipids and contributes to kinds of tissue injuries. However, it remains unclear whether the accumulation of lipid peroxides in UV irradiation-induced skin injury could lead to ferroptosis. We generated UV irradiation-induced skin injury mice model to examine the accumulation of the lipid peroxides and iron. Lipid peroxides 4-HNE, the oxidative enzyme COX2, the oxidative DNA damage biomarker 8-OHdG, and the iron level were increased in UV irradiation-induced skin. The accumulation of iron and lipid peroxidation was also observed in UVB-irradiated epidermal keratinocytes without actual ongoing ferroptotic cell death. Ferroptosis was triggered in UVirradiated keratinocytes stimulated with ferric ammonium citrate (FAC) to mimic the iron overload. Although GPX4 protected UVB-injured keratinocytes against ferroptotic cell death resulted from dysregulation of iron metabolism and the subsequent increase of lipid ROS, keratinocytes enduring constant UVB treatment were markedly sensitized to ferroptosis. Nicotinamide mononucleotide (NMN) which is a direct and potent NAD+ precursor supplement, rescued the imbalanced NAD+/NADH ratio, recruited the production of GSH and promoted resistance to lipid peroxidation in a GPX4-dependent manner. Taken together, our data suggest that NMN recruits GSH to enhance GPX4-mediated ferroptosis defense in UV irradiation-induced skin injury and inhibits oxidative skin damage. NMN or ferroptosis inhibitor might become promising therapeutic approaches for treating oxidative stress-induced skin diseases or disorders.

1. Introduction

Approximately 132,000 cases of malignant melanoma and more than 2 million cases of other skin cancers occur worldwide each year, and epidemiological studies have shown that most skin cancers are caused by overexposure to ultraviolet radiation [1]. Ultraviolet radiation in sunlight is the main source of biological UV exposure on the earth. UV radiation is divided into three wavelength bands: UVA (320–400 nm), UVB (280–320 nm), and UVC (100–280 nm) [2,3]. The atmospheric ozone layer has a strong absorption of UVC, and the UVC reaching the ground is very weak. Approximately 90 to 95% of UVA and 5 to 10% of UVB radiation reaches the ground.

Skin is the largest organ of the human body, composed of epidermis and dermis [4]. Located in the outermost layer of the skin, the epidermis is an important barrier to protect the body from external physical and chemical stimuli and other factors, and these functions are played by keratinocytes. Keratinocytes, which make up more than 90% of epidermal cells, absorb 95% of the ultraviolet light that hits the skin [5]. Moreover, UVB reacts with water in the skin to produce reactive oxygen species (ROS), including singlet oxygen, superoxide anions, and hydroxyl radicals [4,6]. Accumulating evidence suggests that UVB irradiation not only induces nuclear DNA damage but also causes membrane destruction, resulting in cell loss or apoptosis [7,8]. It has been reported that oxidative stress on reactive oxygen species (ROS) produced by UV

^{*} Corresponding authors.

E-mail addresses: gengjie-jie@163.com (J. Geng), liyong0110@hotmail.com (Y. Li), jiaowubio@hotmail.com (J. Wu).

¹ These authors contributed equally to this work.

irradiation is a cause of skin injury [9,10]. Eventually, UV irradiation is expected to cause skin disorders, including skin inflammation, burns, pigment diseases, aging, and skin cancer.

Ferroptosis is a newly discovered iron-dependent programmed cell death mode, which plays an important role in neurodegenerative diseases, tumors, myocardial injury, fibrosis and other diseases, and may also play an important role in skin injury [11,12]. Lipid peroxidation plays an important regulatory role in ferroptosis pathway. Lipid peroxides are the first factor in the occurrence of ferroptosis, and phosphatidylethanolamine (PE) is the preferred substrate for lipid oxidation, so hydrogen peroxide-PE (OOH-PE) is a landmark event in the occurrence of ferroptosis. Glutamate/cystine reverse transporter is an important regulator of ferroptosis, mainly composed of two subunits, 7 member 11 (SLC7A11) and 3 member 2 (SLC3A2) of the transmembrane transporter solute carrier family, which exudes the same amount of glutamate during intracellular cystine transport [13]. By affecting reduced glutathione synthesis, it indirectly affects glutathione peroxidase (GPX4), a core enzyme that regulates ferroptosis. GPX4 catalyzes the reduction of lipid peroxides to reduce OOH-PE to OH-PE using GSH/GSSG redox, thereby inhibiting ferroptosis [14]. The cvst(e)ine/GSH/GPX4 antioxidant axis is one of the most important axes for ferroptosis defense, which is fueled by NADPH. Although lipid peroxidation has been reported as one major effector by which UV contributes to photoaging and skin cancer, it remains unclear if ferroptosis is involved in UV irradiationinduced skin damage.

NMN is synthesized from nicotinamide, a form of water-soluble vitamin B3, and 5'-phosphoribosyl-1-pyrophosphate (PRPP), by NAMPT, the rate-limiting NAD⁺ biosynthetic enzyme in mammals [15–17]. As a key NAD⁺ intermediate, NMN has been shown to enhance NAD⁺ biosynthesis and ameliorate various pathologies in mouse disease models, including aging-related dysfunctions [18]. The administration of NMN, in addition to its anti-aging effects, it will be of great importance to study the effects of NMN administration on the UV induced skin injury.

In this study, we aimed to investigate the accumulation of iron and lipid peroxides and the occurrence of ferroptosis in UV-irradiated skin injury model. The protective effects of ferroptosis inhibition and the underlying mechanism were also investigated. Our results showed NMN can act as a promising therapeutic agent to repair the imbalance of NAD+/NADH ratio and enhance the anti-oxidation function of GSH/GPX4 axis, leading to decrease of the iron-dependent lipid peroxidation and attenuation of UV-induced skin injury.

2. Materials and methods

2.1. Animals

All experimental procedures applied to mice were approved by Ethical Committee of Fourth Military Medical University, and were performed in compliance with the national regulations. BALB/c mice were purchased from the Beijing Vital River Laboratory Animal Technology Co., Ltd. (Beijing, China), and were maintained in a specific pathogen-free mouse facility (room temperature, 20-22 °C; room humidity, 40-60%, with free access to food and water) under a 12-h light/ dark cycle. The skin injury model was created using ultraviolet B (UVB) 250 mJ/cm^2 irradiation onto BALB/c mice after their back shaved. A total of 26 mice were used in this study; 8 mice without treatment served as controls, while 18 mice were irradiated under the UVB lamp and administered with PBS (200 µl per injection area), Lip-1 (Selleck, S7699) (10 mg/kg every other day per injection area), or NMN (Chalet Healthy PTY Ltd, Jiangsu Chengxin Pharmaceutical Co., Ltd) (400 mg/kg/day via drinking water at pH 7.2). One week after injection, blood samples were collected from mice under deep anesthesia, then all the mice were euthanized by an intraperitoneal injection of pentobarbital, and their dorsal skin was collected.

2.2. Cell culture

Human HaCaT cell lines were grown in Dulbecco's Modified Eagle's Mediumor Eagle's Minimum Essential Medium with 10% fetal bovine serum, 2 mM of L-glutamine, and 100 U/mL of penicillin and streptomycin. Cell cultures were maintained at 37 $^{\circ}\mathrm{C}$ in a 5% CO₂ humidified atmosphere.

2.3. Antibodies and western blotting

Antibodies against the following proteins were used in this study: TFRC (1:1000, Abcam ab214039), FPN (1:1000, Abcam ab78066), ferritin (1:2000, Abcam ab75973), HO-1 (1:1000, Abcam ab13243), FSP1 (1:1000, Proteintech 20886-1-AP), HMGB1 (1:1000, Proteintech 66525-1-Ig), ACSL-4 (1:500, Santa Cruz sc271800), SOD2 (1:1000, Santa Cruz sc-133134), CHMP6 (1:1000, Santa Cruz sc-398963), CHMP5 (1:1000, Santa Cruz sc-374337), NRF-2(1:1000, Proteintech 16396-1-AP), SLC7A11 (1:1000, Abcam ab175186), GCLC (1:1000, Abcam ab53179), GCLM (1:1000, Abcam ab126704), GPX4 (1:1000, Abcam ab25066), GAPDH (1:1000, Proteintech 60004-1-Ig). Protein samples were generated using radio immune-precipitation assay (RIPA) lysis buffer (P0013B, Beyotime) with freshly added 1 mM of phenylmethanesulfonyl fluoride (PMSF), protease inhibitors, and phosphatase inhibitors. After that, separated on 10% SDS-polyacrylamide gel, and then the proteins were transferred to a 0.45-µm poly-vinylidene fluoride blotting membranes. The membranes were then incubated with primary antibodies against the proteins of interest in blocking solution, washed and then incubated with HRP-conjugated secondary antibodies. Finally, an enhanced chemiluminescence substrate was added to the membranes prior to film exposure to detect the proteins according to manufacturer's instructions.

2.4. RNA isolation and quantitative PCR

For RT-PCR analysis, tissue RNA was isolated according to purification of RNA using Trizol (TRI reagent) with then reverse transcribed into cDNA with Superscript first strand synthesis kit (Invitrogen) according to the manufacture's protocol. RT-PCR was then performed with a TB Green PCR kit (TaKaRa, Otsu, Japan) on the Mxpro system to determine the expression levels of the genes of interest. All primers were synthesized by the TsingKe Biological Technology (Beijing, China). The sequences of PCR primers are listed in Table 1.

RT-PCR was performed with the following conditions: 95 °C for 3 min; 40 cycles: 95 °C for 15 s, 60 °C for 15 s, 72 °C for 15 s; followed by melting curve analysis. The 2 $^{-\Delta\Delta CT}$ method was used to quantify the relative expression of these genes.

2.5. Enzyme-linked immunosorbent assay (ELISA)

First, samples were generated by western and IP lysis buffer (Beyotime, P0013B), obtain supernatant after centrifuge for 10 min at approximately 12,000 \times g, at 4 °C. CoQ_{10} detection was performed using a CoQ_{10} enzyme-linked immunosorbent assay kit (Sigma-Aldrich, #C9538) according to the manufacturer's instructions. The concentration in each sample well was determined by interpolation from a standard curve. Each sample was tested in triplicate.

2.6. Histology

Tissues were fixed for 24 h in 10% neutral buffered formalin (Sigma), dehydrated in ethanol gradients, paraffin embedded and sectioned at 3 mm on polylysine slides (Thermo scientific). Slides were rehydrated with decreasing percentage of ethanol solutions and subjected to stains.

For hematoxylin and eosin staining, slides were treated for 6 min with Mayer's Hematoxylin (Sigma Aldrich), rinsed in phosphate buffered saline, and incubated for 2 min in Eosin in acetic acid (Sigma

 Table 1

 Primer sequences for real-time quantitative PCR.

Real-time quantitative PCR Mouse primers	GAPDH	Forward 5'-ATCATCCCTGCATCCACT-3'
		Reverse 5'-ATCCACGACGGACACATT-3'
	TFRC	Forward 5'-
		CTCAGTTTCCGCCATCTCAGT-3'
		Reverse 5'-
		GCAGCTCTTGAGATTGTTTGCA-3'
	FPN	Forward 5'-
		GTGGAGTACTTCTTGCTCTGG -3'
		Reverse 5'-
		CTGCTTCAGTTCTGACTCCTC-3'
	FTH	Forward 5'-
		CCATCAACCGCCAGATCAAC-3'
		Reverse 5'-
		GAAACATCATCTCGGTCAAA-3'
	FTL	Forward 5'-
		CGTCTCCTCGAGTTTCAGAAC-3'
		Reverse 5'-
		CTCCTGGGTTTTACCCCATTC-3'

Aldrich). After the stains, slides were dehydrated with ethanol gradients and mounted with Entellan (Sigma Aldrich). Digital images were acquired up to $4\times$ or $20\times$ magnification.

For Masson's trichrome staining, slides were treated overnight with the Bourin's mordent solution (Roth). After washing, slides were treated for 5 min with Weigert's hematoxylin (Roth), 5 min with Biebrich Scarlet Acid Fuchsine (Sigma Aldrich), 5 min with Phosphotungstic/Phosphomolybdic Acid Solution (Sigma Aldrich), 5 min with Aniline Solution (Sigma Aldrich) and 2 min with 1% acetic acid (Carl Roth).

Immunohistochemical staining was performed using a streptavi-din–peroxidase kit (ZSGB-Bio, China). The primary antibodies targeted the following proteins or modifications: 4-hydroxynonenal (Abcam, ab48506), PTGS2(Abcam, ab179800), 8-Hydroxy-2'-deoxyguanosine (Abcam, ab48508), HO-1 (Abcam, ab13243), transferrin receptor (Abcam, ab214039), and ferritin (Abcam, ab75973), with a standard avidin-biotin HRP detection system according to the instructions of the manufacturer (anti-mouse/rabbit HRP-DAB Cell & Tissue Staining Kit, R&D Systems Minneapolis, MN). Tissues were counterstained with hematoxylin, dehydrated, and mounted. Quantitative analysis was performed with Image-Pro Plus Version 6.0 software.

2.7. Measurement of cell death, ROS and lipid peroxidation

Experiments were performed according to the manufacturer's protocol. Cell death was analyzed by SYTOX Green (Invitrogen) staining followed by microscopy or flow cytometry. Briefly, cells were incubated in a humidified chamber at 37 $^{\circ}\text{C}$ with 5% CO $_2$ for 30 min with Lipid Peroxidation Sensor or CM-H2DCFDA in cell culture medium. After incubation, cells were washed and examined by flow cytometry within 2 h of staining.

2.8. Measurement of serum iron level and cellular iron staining

Total iron levels in serum samples of BALB/c mice were assessed by the Iron Assay Kit (Abcam, ab83366) according to the manufacturer's instructions. In brief, an iron reducer was added to the sample and standard wells. The mixture was incubated at 37 $^{\circ}\text{C}$ for 30 min, and iron was added and incubated for an additional 60 min. The output was then immediately assessed on a colorimetric microplate reader (OD =593 nm).

Cells were washed with PBS twice and stained with 10 nM of Phen Green SK for 15 min in 37 $^{\circ}$ C. After staining, cells were centrifuged and re-suspended in PBS and the fluorescence profile of the sample was monitored using a BD aka Fortessa X30 system. Higher fluorescence intensity indicates lower iron level.

2.9. NAD+/NADH and NADP+/NADPH measurement

Cellular NAD $^+$ /NADH measurement was performed using the manufacturer's protocol (Beyotime, S0175). Cellular NADP $^+$ /NADPH measurement was performed using the manufacturer's protocol (Beyotime, S0179).

2.10. Quantification of GSH

Cells were treated as indicated, and cellular GSH levels were assessed using the GSH- GSH/GSSG Ratio Detection Assay Kit (Abcam, ab138881) following the manufacturer's instructions. In brief, the GSH assay mixture was added to the whole-cell lysates for a one-step fluorometric reaction and incubated for 60 min while protected from light. Fluorescence was then monitored at EX/EM wavelengths of 490/520 nm, and reduced GSH was calculated from the standard curve. The reduced GSH concentration in each group was normalized to cell viability.

2.11. RNAi and gene transfection

The human GPX4-shRNA#1 (5'-GGAGTAACGAAGAGATCAAAG-3'), human GPX4-shRNA#2 (5'-GGATGAAGATCCAACCCAAGG-3'), and control empty shRNA were obtained from GenePharma Co. Ltd. (Suzhou, China). Human RNAi and gene transfection were performed using Lipofectamine2000 (Thermo Fisher Scientific) according to the manufacturer's instructions.

2.12. Statistical analysis

The experiments were performed independently at least three times. The data were expressed as mean value \pm SD. Unpaired and paired t-tests or one-way analysis of variance followed by Dunnett's posttest (for subgroup analyses) was used. All of statistical images were processed by Graph Pad Prism 8.0 software. Differences were considered to be statistically significant when p < 0.05.

3. Results

3.1. UV irradiation-induced skin damage involves the accumulation of lipid peroxides and iron overload

The skin injury model was successfully created using ultraviolet (UV) 250 mJ/cm² irradiation onto BALB/c mice after their back shaved. UV induced subcutaneous swelling and epidermal hyperplasia (Fig. 1A), and the changes of histological properties in control and UV group were examined. First, hematoxylin-eosin (HE) staining results showed that UV irradiation resulted in an increase of epidermal and dermal thickness in comparison to sham group at 7 d (Fig. 1B, D—F). Second, the plastic state of the collagen fibers was examined using Masson's trichrome staining in each group, statistical analysis showed that UV group increased the density of the collagen fibers (collagen area%) (Fig. 1C, G). We then used immunohistochemistry to measure two putative biomarkers of oxidation and lipid peroxidation in mice skin tissues, 8-Hydroxy-2'-deoxyguanosine (8-OHdG) and 4-hydroxynonenal (4-HNE) modifications (Fig. 2A, B) [19,20]. We found an increased staining for 4-HNE and 8-OHdG in the injured skin tissues of mice subjected to UV injury compared to non-treated mice, indicating increased levels of lipid peroxidation. A significant increase of transferrin receptor (TFRC) expression along with a significant increase of ferritins (heavy and light chains) was observed in skin tissues with UV irradiation, implying the enhancement of iron uptake and storage. In addition, the expression of the iron related genes in dorsal skin was detected using qPCR. In line with the above results, we observed that the mRNA levels of TFRC, FTL, FTH were increased in UV group, whereas the mRNA level of the unique iron exporter ferroportin (FPN) was decreased compared to that in the

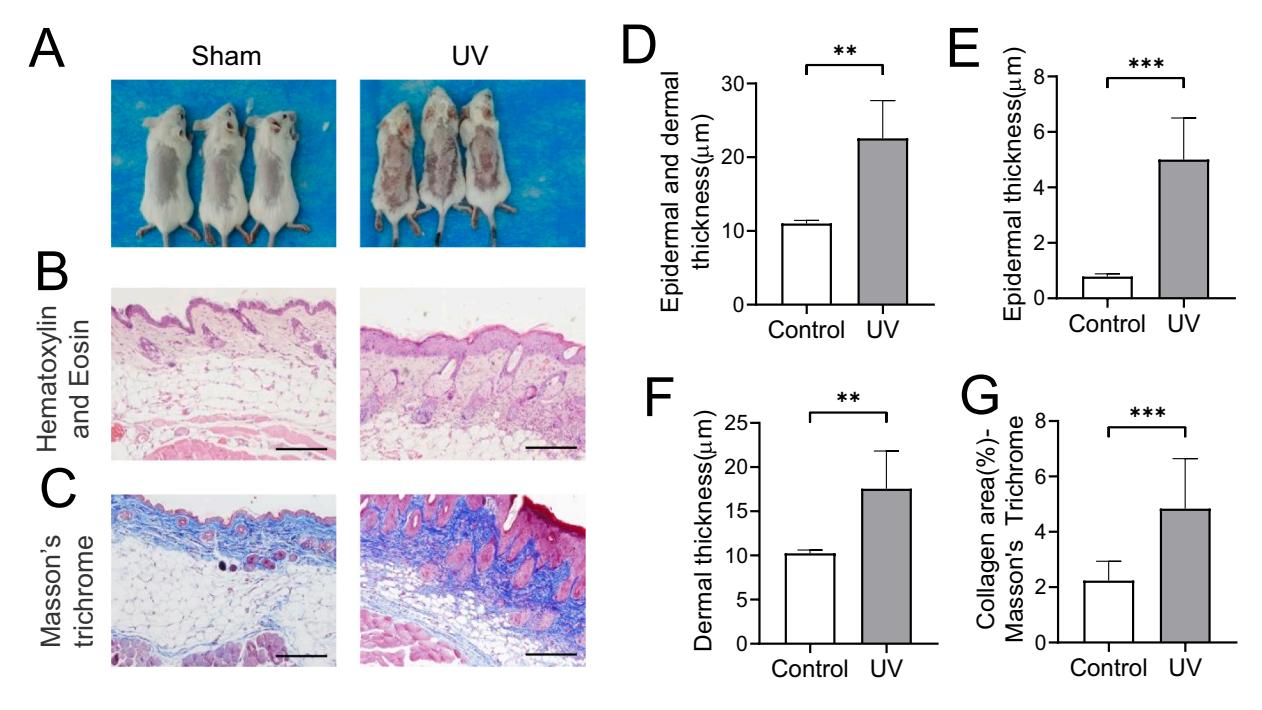


Fig. 1. UV-induced histological injury in mice skin. After UV-irradiated mice, the histological changes were examined in this study. (A) Representative photos present the morphological change of dorsal skin in each group at 7 d post-UV irradiation. (B, C) Representative images present Hematoxylin-eosin (HE), Masson's Trichrome of mice skin in Sham, UV group at 7 d post-UV irradiation. (D-G) Quantification of the epidermal and dermal thickness (D), the epidermal thickness (E), dermal thickness (F) and relative collagen area (%) (G) in the experimental groups is shown. Horizontal bars in all histograms denote the statistical significance between groups. P values were determined by one way-ANOVA. Scale bars: B and C, 10 μm; n = 3 per group. p = 3 per group

non-treated group (Fig. 2C). Iron assay showed that serum ${\rm Fe}^{2+}$ concentration increased in UV group mice (Fig. 2D). These results indicate that the accumulation of lipid peroxides and iron overload in UV-induced skin damage.

3.2. Keratinocytes show anti-ferroptosis phenomenon after UVB irradiation

To determine the role of lipid peroxidation and iron in the development of skin damage, we irradiated human keratinocytes (HaCaT cells) with increasing doses of UVB light in the range of 15 mJ/cm²–200 mJ/cm² for once or three times. Cytoplasmic ROS production, lipid ROS and iron level were accessed in living cells by flow cytometry. The sensor in the lipid peroxidation kit changes its fluorescence from PE to FITC upon peroxidation by lipid ROS in cells, thus enabling ratio metric measurement of lipid peroxidation (the decreasing PE/FITC ratio means increasing lipid peroxidation). For Fe²⁺ detection, higher fluorescence intensity means lower iron level. Although one-time UVB irradiation effectively increased the intracellular ROS generation and nonheme iron levels, it failed to promote the accumulation of lipid peroxides (Fig. 3A-C). After three times UVB irradiation, the ROS level increased up to -55folds in HaCaT cells irradiated with 200 mJ/cm² UVB compared with the control, which is much higher than the ROS production induced by one-time irradiation (Fig. 3D). Cells with three times UVB irradiation also showed remarkable increase of lipid peroxidation and higher iron level (Fig. 3E-F). Since increase of intracellular lipid ROS generated by excess iron could probably lead to ferroptosis, we measured the percentage of dead cells using SYTOX staining. Surprisingly, there was no significant cell death in HaCaT cells irradiated with repeated UVB irradiation (Fig. 4A). These results imply the existence of cellular defense mechanisms against ferroptosis in UVB-injured keratinocytes.

3.3. GPX4 protects UVB-injured keratinocytes against the accumulation of lipid ROS resulted from dysregulation of iron metabolism

Several proteins have been shown to maintain iron homeostasis by regulating iron absorption, transport, and storage. Iron absorption is mainly controlled by the plasma membrane protein TFRC and stored within ferritin, and cellular iron export is mediated by FPN. As shown in Fig. 4B-4D, one time UVB irradiation increased the expression of both TFRC and FPN while three times UVB irradiation increased the expression of TFRC but decreased the expression of FPN in keratinocytes HaCaT cells. The dysregulation of iron metabolism resulted to increased uptake and decreased export of iron, leading to iron overload in chronic UVB-injured keratinocytes. One time or three times UVB irradiation is expected to stimulate many antioxidation molecules help to protect normal skin cells from UVB injury. Anti-oxidant enzymes or membrane repair machinery to resist to ROS cytotoxicity, including SOD2, CHMP5, CHMP6, NRF-2 were all upregulated in response to one time UVB irradiation (Fig. 4B). These antioxidant molecules failed to increase in keratinocytes with three times UVB irradiation (Fig. 4C), which is likely to represent the disruption of the adaptive cellular response that attempts to suppress oxidative injury. As one of the major ferroptosis and lipid ROS defense systems, GPX4 is upregulated in response to both one time and three times UVB irradiation (Fig. 4B, C). Overall, these data indicate that GPX4 might be involved in the ferroptosis defense against lipid ROS accumulation resulted from iron overload in the UVB-injured keratocytes.

3.4. The NAD $^+$ precursor supplement NMN recruits GSH production and suppresses the production of lipid peroxides via GPX4

We then used ferric ammonium citrate (FAC) to treat UVB-induced HaCaT cells to mimic the iron overload. Compared to one-time exposure to UVB irradiation, repeated exposure in combination with FAC induced substantial cell death, which could be largely rescued by deferoxamine (DFO, an iron chelator) and ferrostatin-1 (Fer-1, a

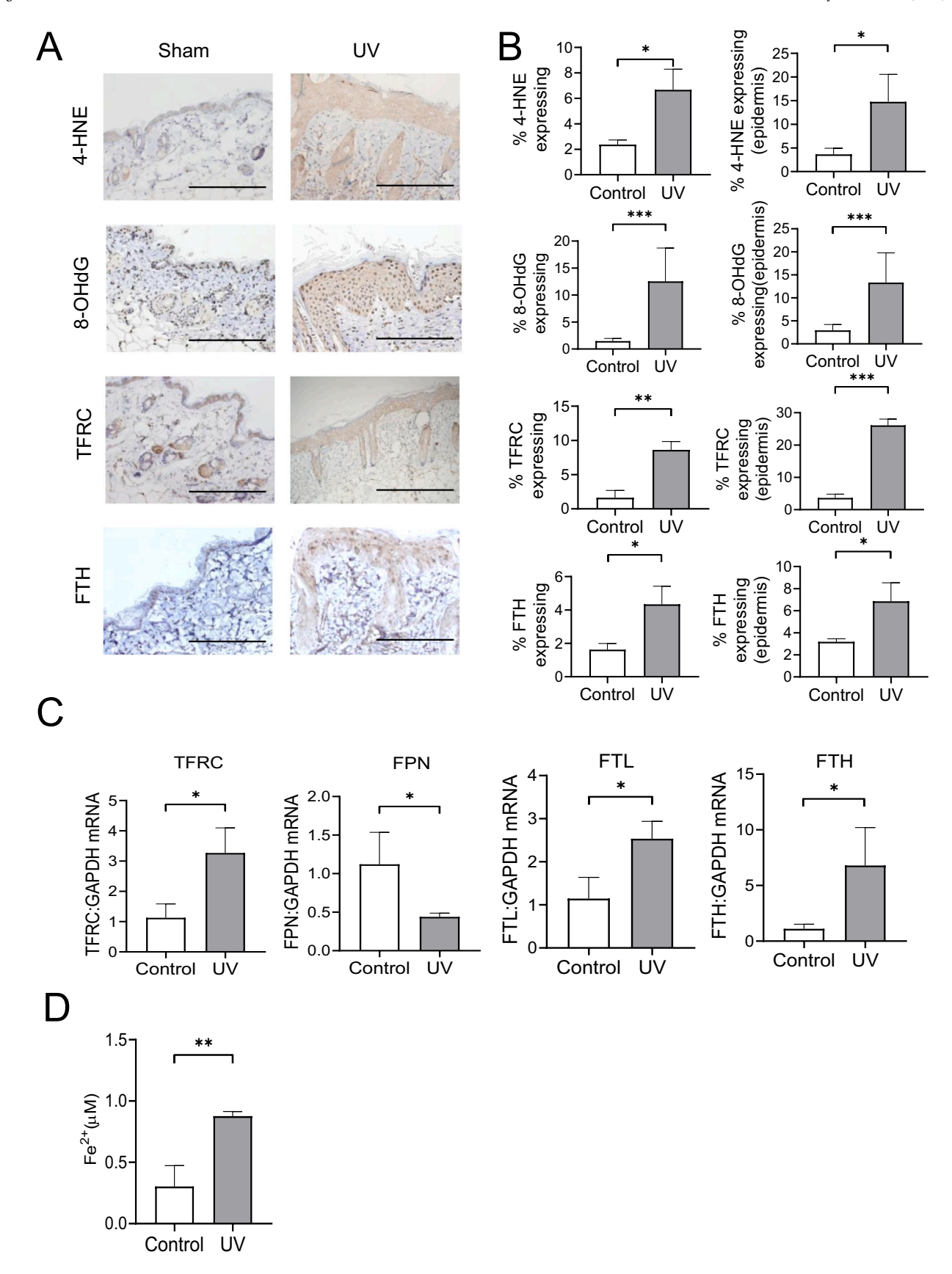


Fig. 2. Iron and lipid peroxidation accumulated in mice dorsal skin after UV-irradiation. (A) Representative images of 4-HNE, 8-OHdG, TFRC and FTH in dorsal skin of the Sham, UV group at 7 d post-UV irradiation. (B) Quantification of the expression of 4-HNE, 8-OHdG, TFRC and FTH (n=3 per group) in the experimental groups is shown. (C) qPCR of the RNA levels of TFRC, FPN, FTL and FTH in dorsal skin tissue of the experimental groups (n=3 per group) at 7d post-UV irradiation. (D) The histograms show the concentration of ferrous ion in serum of each group (n=3 per group) at 7 d post-UV irradiation. Horizontal bars in all histograms denote the statistical significance between groups. P values were determined by one way-ANOVA. Scale bars: A, 10 μ m. *p < 0.00; **p < 0.01; ***p < 0.001.

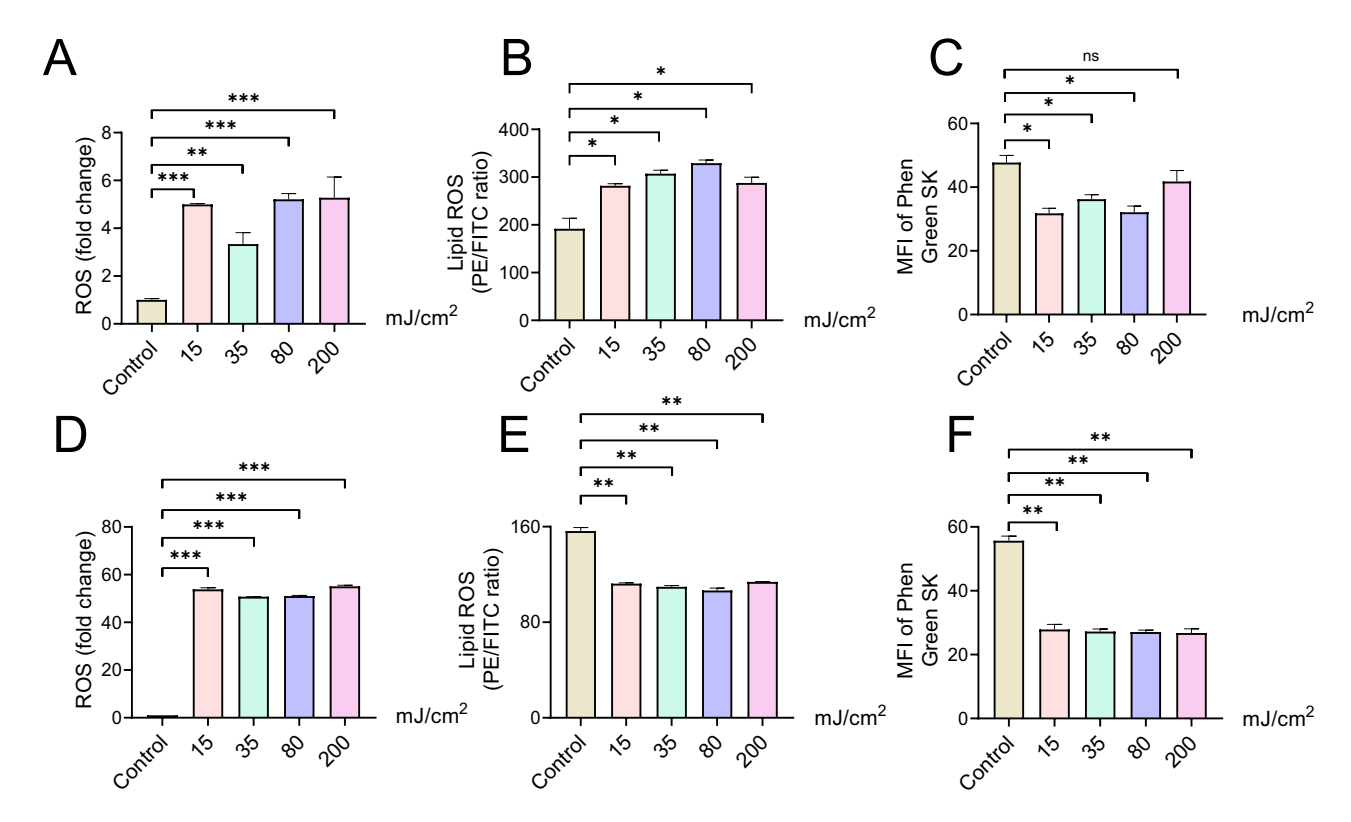


Fig. 3. UVB induced injury regulate metabolic programs, including ROS, lipid peroxidation, iron in HaCaT cells. (A-F) HaCaT cells were analyzed for ROS (A), lipid peroxidation (B), iron (C) after UVB induced injury. HaCaT cells were analyzed for ROS (D), lipid peroxidation (E), iron (F) after UVB induced injury. Horizontal bars in all histograms denote the statistical significance between groups. P values were determined by one way-ANOVA. *p < 0.05; **p < 0.01; ***p < 0.001; ns, none significant. HaCaT, human keratinocyte.

ferroptosis inhibitor) (Fig. 5A). Consistently, FAC-induced potent lipid peroxidation in HaCaT cells treated with repeated UVB irradiation could be partially inhibited by DFO or Fer-1 (Fig. 5B-C). These results demonstrate that although keratocytes treated with both one-time and repeated UVB irradiation exhibited resistance to the ferroptotic damage, cells enduring constant UVB treatment were markedly sensitized to ferroptosis induced by intracellular iron overload. To explore the underlying mechanisms modulating ferroptosis resistance, we detected the NAD+/NADH ratio, which as shown in Fig. 5D and E, redox balance NAD+/NADH was disrupted in FAC treated group but returned to normal level when cells were stimulated by Fer-1 in HaCaT cells with three times UVB irradiation induced skin injury (Fig. 5D, E), NMN, which is a direct and potent NAD⁺ precursor supplement, effectively healed NAD⁺/NADH redox imbalance (Fig. 5F), increased the cytosolic level of NADPH (Fig. 5G), inhibited cell death (Fig. 5H) and attenuated the lipid peroxidation level (Fig. 51). Importantly, the decreased GSH level induced by FAC was significantly rescued by NMN or Fer-1

Interestingly, we found the expression of GPX4 was increased in FAC + NMN group compared to the control group and FAC group (Fig. 6A). To determine whether NMN regulates ferroptosis through enhancing the function of GPX4 in UVB induced skin injury, we first suppressed GPX4 expression by specific shRNA. Western blot confirmed an effective reduction of GPX4 expression (Fig. 6B). Importantly, the knockdown of GPX4 increased cell death in response to UVB irradiation and FAC stimuli (Fig. 6C). GPX4 inhibit ferroptosis by transferring glutathione (GSH) to oxidized glutathione (GSSG) using NAD+/NADH system. NAD+ declined could be reversed through treatment with the NAD+ precursor NMN [21]. Compared to its effect on control shRNA cells, NMN failed to diminish the accumulation of lipid ROS and cell death of GPX4-konckdown HaCaT cells, which was in line with decreased GSH level in the UVB radiation and iron overload (Fig. 6D, E).

3.5. NMN and liproxstatin-1 strongly mitigated UV-induced skin injury

Next, we investigated the therapeutic effects of NMN and liproxstatin-1 on oxidative skin injury in mice. At the same time UVinduced subcutaneous swelling and epidermal hyperplasia (Fig. 7A). Hematoxylin & Eosin staining results showed that NMN or liproxstatin-1 treatment significantly reduced the increase of epidermal and dermal thickness at 7 d post-UV irradiation (Fig. 7B, C). The plastic state of the collagen fibers was examined using Masson's trichrome staining in each group, statistical analysis showed that NMN or liproxstatin-1 treatment failed to decrease the density of the collagen fibers (collagen area%) presented in UV group (Fig. 7B, D). In NMN treatment group, it shows decrease in 4-HNE, COX2, 8-OHdG, and HMOX-1 expression level (Fig. 8A), there is statistical difference of 4-HNE, COX2, 8-OHdG, and HMOX1 between UV + NMN and UV groups (Fig. 8B, C, D, E). And also, the serum 8-OHdG level was decreased after NMN administration (Fig. 8F). However, neither liproxstatin-1 nor NMN inhibited the increased expression of TFRC, ferritin, and serum Fe2+concentration induced by UV irradiation (Fig. 7E, F, G, H). Collectively, these results suggest that NMN and liproxstain-1 can attenuate UV induced histological injury in mice skin by resisting to lipid peroxides. Mechanistically, our data support a model in which UV irradiation-induced skin injury leads to the accumulation of cellular iron and lipid peroxides. Although activated GPX4 suppresses ferroptotic cell death, it cannot completely block the propagation of lipid peroxides due to the ruin of NAD+/NADH redox loop and GSH recruitment process. NMN markedly rescues the imbalance of NAD+/NADH and attenuates the accumulation of lipid peroxidation to weaken the repeated UV irradiation-induced skin injury (Fig. 8G).

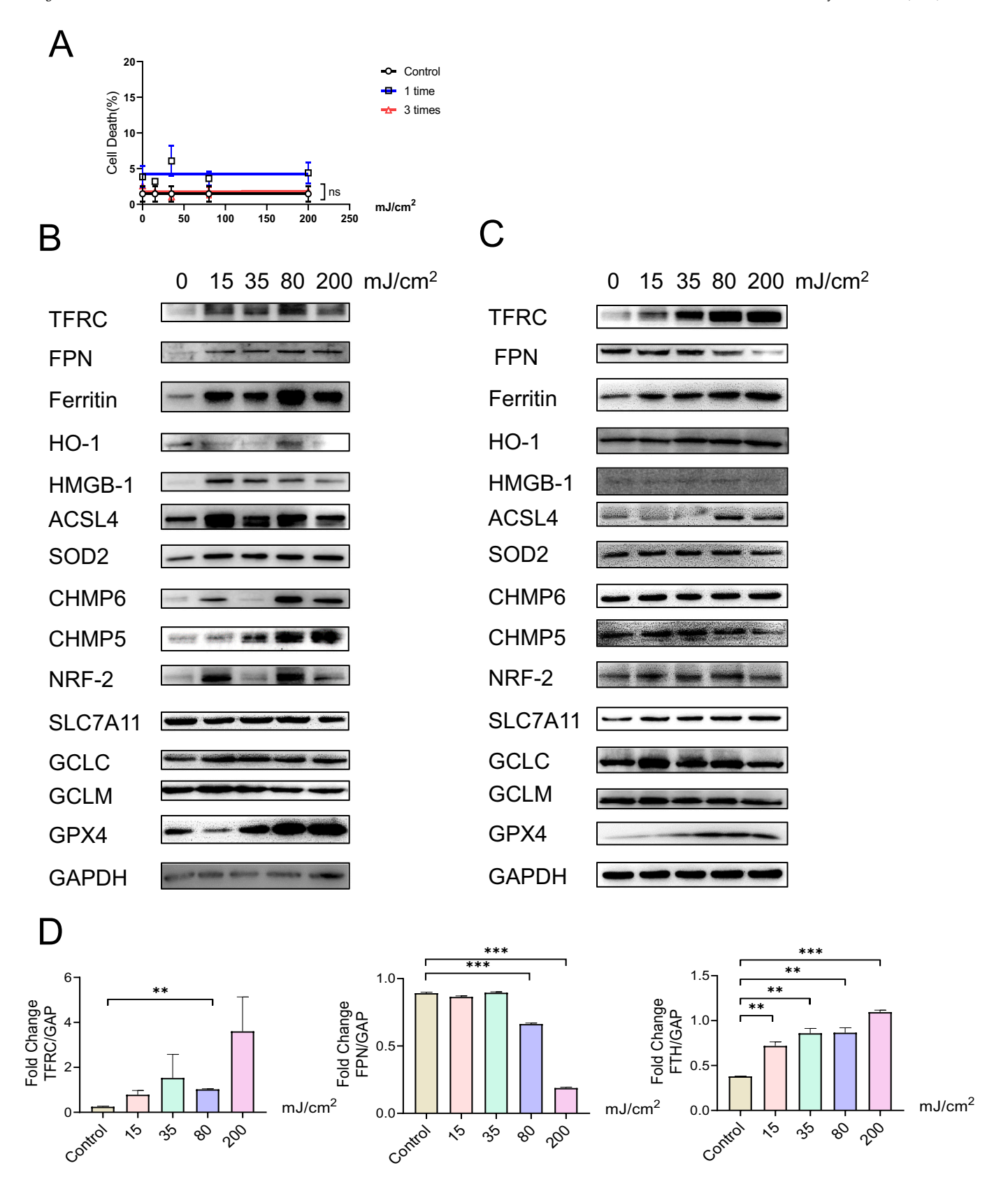


Fig. 4. UVB irradiation activates antioxidant activity and ease oxidative response. (A) Cell death ratio were detected in control, UVB induced injury group post 1 time and 3 times UV irradiation. (B, C) The iron related proteins and anti-oxidant molecules were further determined by Western blotting after UVB induced injury. (D) Quantification of gray value shows the relative expression (/gapdh) of iron-related proteins, including TFRC, FPN, FTH (n=3 per group). Statistical difference between groups is shown in all histograms. P values were determined by one way-ANOVA. *p < 0.05; **p < 0.01; ***p < 0.001; ins, none significant.

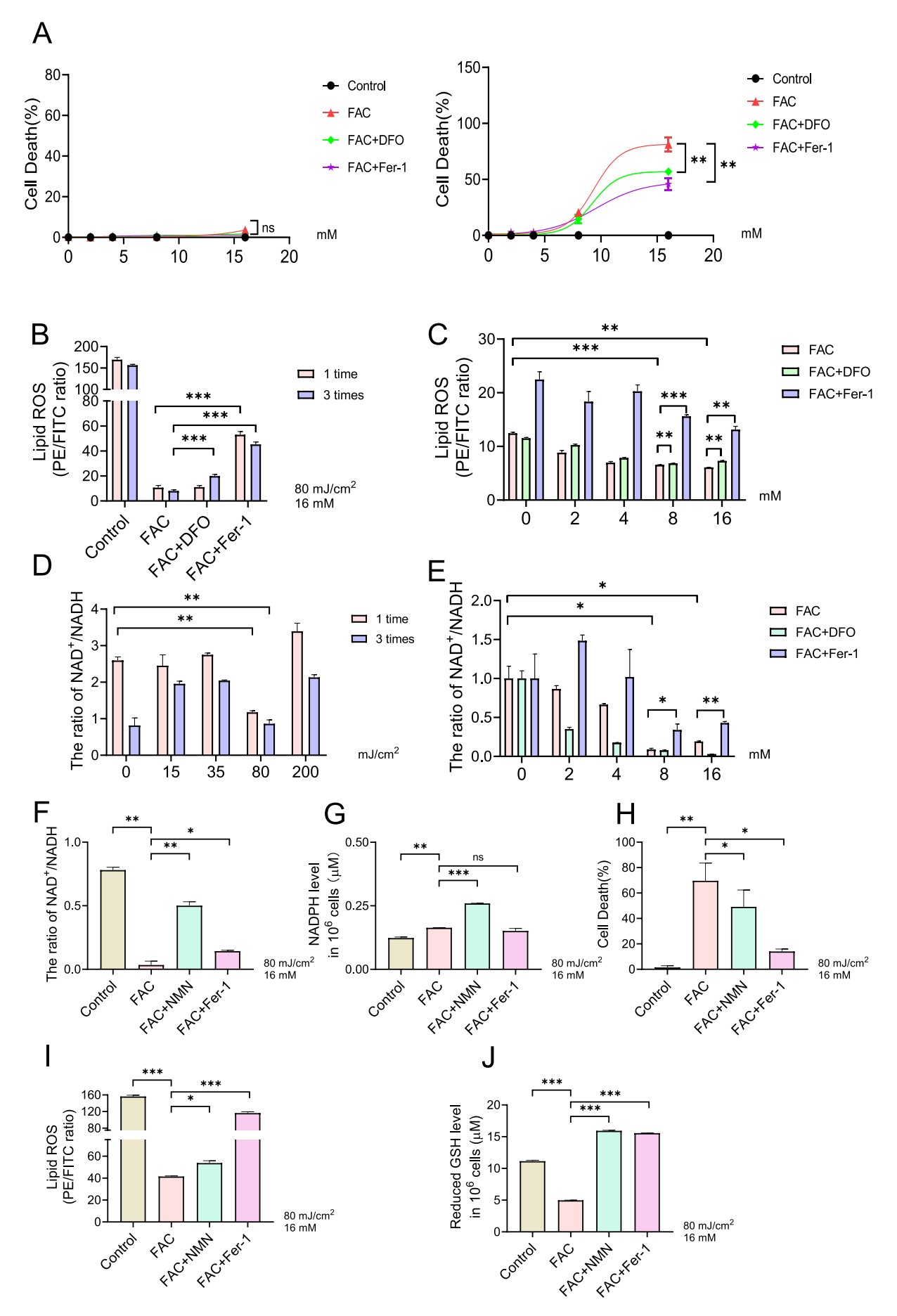


Fig. 5. NMN generates NAD $^+$ to increase GSH level in HaCaT cells after UVB irradiation and iron overload. (A) Analysis of cell death in HaCaT cells following treatment with FAC (16 mM), DFO (50 mM), or Fer-1 (1 mM) after UVB induced injury. (B) Lipid peroxidation were detected in HaCaT cells following treatment with FAC (16 mM), DFO (50 mM), or Fer-1 (1 mM) after UVB induced injury. (C) Lipid peroxidation were detected in HaCaT cells following treatment with DFO (50 mM), or Fer-1 (1 mM) at different FAC concentration point. (D) NAD $^+$ /NADH ratio were detected in HaCaT cells after UVB induced injury in different intensity. (E) NAD $^+$ /NADH ratio were detected in HaCaT cells were analyzed lipid peroxidation (F), NADPH level (G), cell death (H), NAD $^+$ /NADH ratio (I), and GSH level (J) following treatment with FAC (16 mM), NMN (20 mM), or Fer-1 (1 mM) after UVB (80 mJ/cm 2) induced injury. Statistical difference between groups is shown in all histograms. *P* values were determined by one way-ANOVA. *p < 0.05; **p < 0.01; ***p < 0.001; ns, none significant.

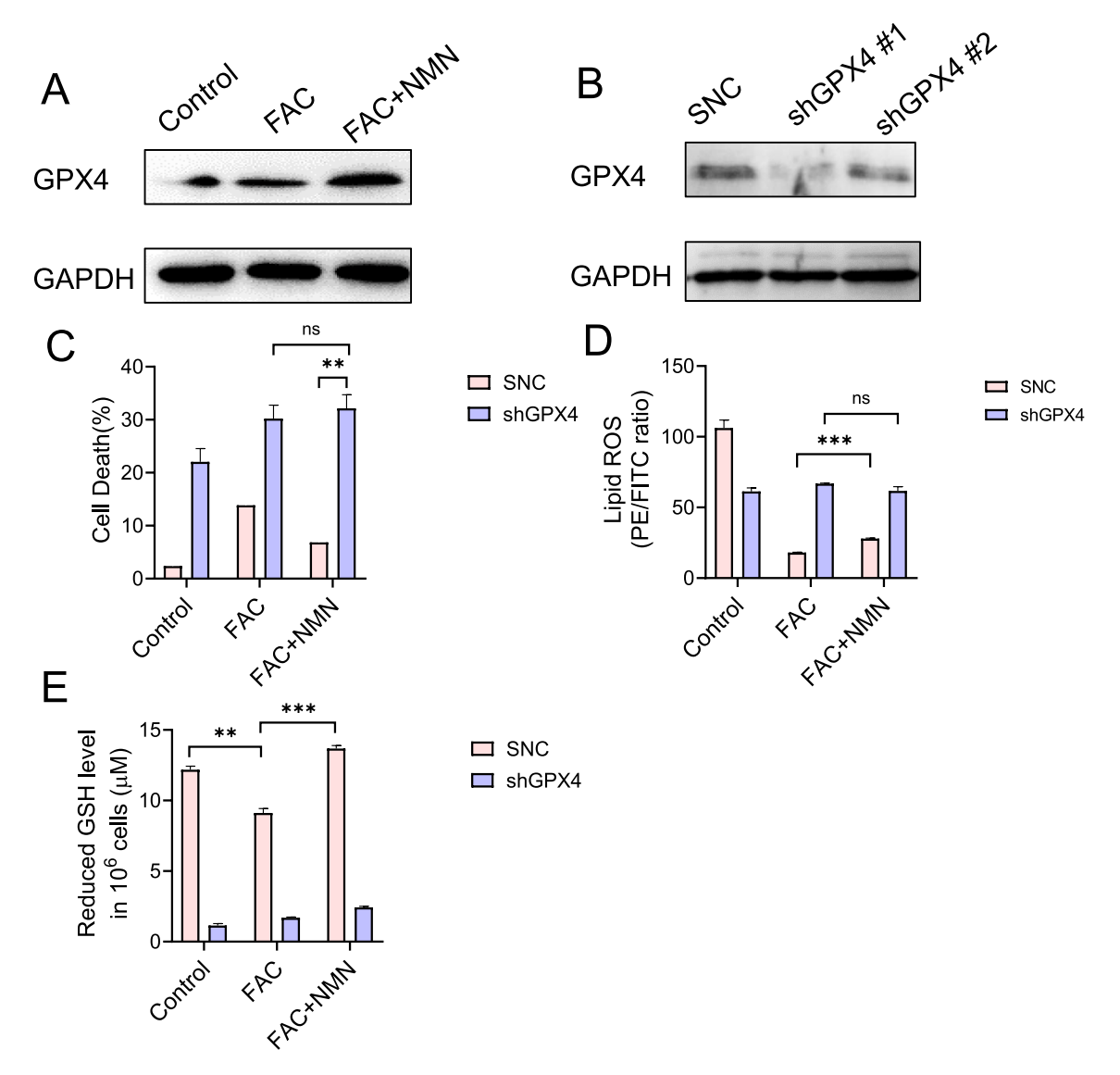


Fig. 6. NMN recruitment GSH to enhance GPX4 resistance to ferroptosis in HaCaT cells after UVB irradiation and iron overload. (A) The expression of GPX4 protein was detected by Western blotting in HaCaT cells following treatment with NMN (20 mM) after UVB irradiation and iron overload stimulus. (B) Western blot analysis of GPX4 protein expression in control and GPX4-knockdown HaCaT cells. (C-E) Analysis of cell death (C), lipid peroxidation (D), GSH level (E) in control and GPX4-knock down HaCaT cells following treatment with FAC (16 mM) or NMN (20 mM) after three times UVB irradiation induced skin injury. Statistical difference between groups is shown in all histograms. P values were determined by one way-ANOVA. *p < 0.05; **p < 0.01; **p < 0.001; ns, none significant.

4. Discussion

UV-radiations are the invisible part of light spectra having a wavelength between visible rays and X-rays. Based on wavelength, UV rays are subdivided into UV-A (320–400 nm), UV-B (280–320 nm) and UV-C (200–280 nm). Ultraviolet radiation can give rise to many chronic skin conditions, including skin cancer, which is now the most common type of cancer worldwide [1]. Oxidative stress is a major cause of skin injury induced by UV radiation. The consequences of UV exposure are

implicated in skin aging and cell death.

As an essential trace element, iron plays an important role in a wide range of key biological processes in all living organisms. According to its ability to switch between specific oxidative forms, iron is an important co-factor in the electron transfer process and in oxidation–reduction reactions [22]. On the other hand, iron's redox potential also contributes to cellular toxicity during iron overload. Ferroptosis is a recently described form of regulated cell death which is iron and lipid oxidation products-dependent. Ferroptosis can occur by different pathways, then

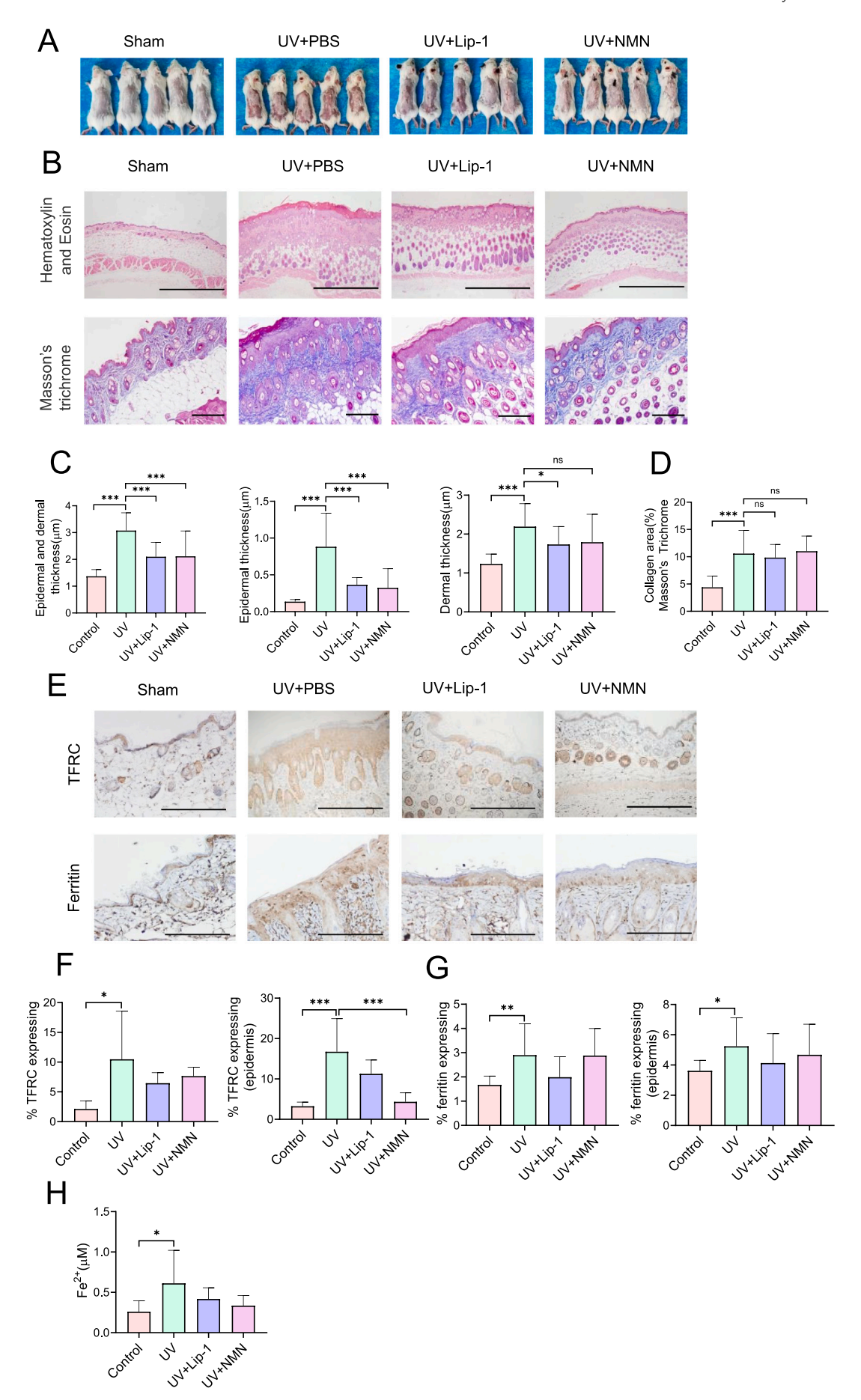


Fig. 7. NMN significantly attenuated the severity of UV-induced histological injury in mice skin. (A) Representative photos present the morphological change of dorsal skin in each group at 7 d post-UV irradiation. (B) Representative images present Hematoxylin-eosin (HE), Masson's Trichrome of mice skin in Sham, UV, UV + Lip-1, and UV + NMN 4 groups at 7 d post-UV irradiation. (C, D) Quantification of the epidermal and dermal thickness(left), the epidermal thickness (medium), dermal thickness (right) and relative collagen area (%) (D) in the experimental groups is shown. (E) Representative images of TFRC, ferritin in dorsal skin of the Sham, UV, UV + Lip-1, and UV + NMN 4 groups at 7 d post-UV irradiation. (F, G) Quantification of the expression of TFRC and ferritin in the experimental groups is shown. (H) The histograms show the concentration of ferrous ion in serum of each group (n = 5 per group) at 7 d post-UV irradiation. Horizontal bars in all histograms denote the statistical significance between groups. P values were determined by one way-ANOVA. Scale bars: A and E, 10 μm; n = 3 per group. *p < 0.05; **p < 0.01; ***p < 0.001; ns, none significant.

displays morphological patterns of necroptosis, including membrane rupture and cell content release [23,24]. The dysregulation of iron homeostasis is a key component of ferroptosis machinery. The level of Fe²⁺ reflects the iron overload that can generate highly reactive hydroxyl radicals through the Fenton reaction. Iron metabolism dysfunction and ferroptosis has been proven to be involved in diverse forms of tissue injuries in brain, heart, liver and kidney, including heart ischemiareperfusion (I/R) injury, ischemia stroke, intracerebral hemorrhage, acute kidney injury, and liver fibrosis [25-27]. In UV irradiation, it has been reported that UV irradiation increases ferrous iron release [28]. Our results showed that in UV-irradiated skin injury mice model and human skin keratinocytes, iron was overloaded and lipid peroxides were accumulated without actual ongoing ferroptotic cell death. In our research, there are some iron related molecules that have changed during the UV-radiation process, including TFRC, ferritin, and FPN. A significant increase of TFRC expression along with a significant increase of ferritins (heavy and light chains) was observed in skin tissues after UV irradiation, implying the enhancement of iron uptake and storage. In addition, the expression of the iron related genes in dorsal skin was detected using qPCR. In line with the above results, we observed that the mRNA levels of TFRC, FTL, FTH were increased in UV group, whereas the mRNA level of the unique iron exporter ferroportin (FPN) was decreased compared to that in the non-treated group. Iron assay showed that serum Fe²⁺ concentration increased in UV group mice. These results indicate that the accumulation of lipid peroxides and iron overload in UV-induced skin damage.

In keratinocytes irradiated with one-time UVB, we found there was an increase of anti-oxidant molecules, including SOD2, CHMP5, CHMP6, NRF-2. But in keratinocytes receiving repeated UVB irradiation, these anti-oxidant molecules remained unchanged and cells showed increased susceptibility to iron accumulation. Interestingly, the level of a key inhibitor of ferroptosis, GPX4, increased regardless of the frequencies of UVB irradiation. Genetic inactivation of GPX4 resulted in death of mice around embryonic day 7.5, likely from defects in brain development [29]. Inactivation of GPX4 in post-natal mice is sufficient to promote lethal, acute renal failure, suggesting an important homeostatic role for this protein in the developing kidney. Tissue-specific disruption of GPX4 can also lead to the destruction of muscle, neuronal and other cells, indicating a broad requirement for GPX4 in the survival of many adult cells. Although the upregulation of GPX4 protected keratinocytes from ferroptosis induced by repeated UVirradiation, GPX4 failed to defend lipid ROS accumulation and ferroptotic cell death when UV-injured keratinocytes were further pressurized with iron overload. Therefore, we hypothesize that the enzymatic function of GPX4 was partially damaged by the oxidative injury resulted from UV-irradiation. To prove this hypothesis, we investigated the mechanism of GPX4 regulation of ferroptosis. As an important reduction product in the body, GSH is the only substrate of GPX4. GPX4 reduced GSH to oxidized glutathione (GSSG) to eliminate the peroxide production on membrane lipids and block the damage of cell membranes, thus inhibiting the occurrence of ferroptotic cell death. The cystine/glutamate antiporter SLC7A11 functions to import cystine for GSH biosynthesis. Apart from this, GSH could also be restored from GSSG by glutathione reductase (GR) under consumption of NADPH as a source of reducing equivalents. Due to the pivotal importance of cytosolic NADPH in ferroptosis for nourishing GSH-dependent system, the basal level of NADPH has proven to be a biomarker of ferroptosis sensitivity, and

NADPH depletion by a cytosolic NADPH phosphatase facilitates ferroptosis in several cancer cell lines [30,31]. NADPH could be generated by several routes such as the pentose phosphate pathway (PPP), NAD kinase (NADK)-catalyzed phosphorylation of NADH, and the conversion of isocitrate to a-KG by NADP-dependent isocitrate dehydrogenase (IDH) [32].

NMN, Nicotinamide mononucleotide, is a substance inherent in the human body and is also found in some fruits and vegetables. The administration of NMN has been shown to mitigate aging-related dysfunctions [18]. Long-term NMN administration prevents age-associated loss of the neural stem/progenitor pool in the dentate gyrus in wild-type C57BL/6 mice [33]. In human body, NMN is the precursor of NAD⁺, and its function is embodied by NAD⁺. Due to the large molecular weight and unstable structure of NAD⁺, the human body cannot directly absorb NAD⁺. It has been scientifically proved that direct oral administration of NMN products is the best way to supplement NAD⁺. In the cytosol, NADP(H) is derived from nicotinamide adenine dinucleotide [NAD(H)] by NAD kinase (NADK) [34]. Both NADH and NADPH serve as hydrogen and electron donors for transferring glutathione (GSH) to oxidized glutathione (GSSG) reactions to inhibit ferroptosis inside the cell [35].

Evidence accumulating from studies conducted in rodents has demonstrated that systemic NMN administration effectively enhances NAD⁺ biosynthesis in various peripheral tissues, including pancreas, liver, adipose tissue, heart, skeletal muscle, kidney, eyes, and blood vessels [36-42]. Previous studies demonstrate that restoration of NAD⁺ levels by NMN treatment exert protective effects in aged rodents by reducing ROS generation and restoring mitochondrial function in a sirtuin-dependent manner [43]. Also, NMN treatment during I/R injury markedly restored the reduced NAD+/NADH ratio to levels similar to the uninjured group [44]. Our data showed that NMN treatment effectively normalized the NAD+/NADH redox balance during UV irradiation-induced injury of keratinocytes, in line with the restoration of GSH. The NAD⁺/NADH redox plays a crucial role in regulating the intracellular redox state, whose imbalance resulted in dysregulated cellular metabolism [45]. Furthermore, we found that NMN treatment increased the expression of GPX4 in keratinocytes after UVB irradiation and iron overload, which further enhanced the anti-ferroptosis GSH/ GPX4 axis, inhibited the accumulation of lipid ROS and attenuated the skin damage caused by UV irradiation. We found NMN failed to inhibit the increase of cell death and lipid ROS level upon UV-irradiation and iron overload in GPX4-knockdown keratinocytes, demonstrating that NMN-mediated ferroptosis defense is dependent on GPX4. These results indicated that in addition to the anti-aging effect of NMN, it will be of great importance to study the effects of NMN administration on the UV induced skin injury. The anti-aged effects of NMN may play a key role in maintaining skin health, as well as preventing UV-induced skin damage and skin carcinogenesis.

Taken together, the present study indicates that UV irradiation increased the iron accumulation and lipid peroxidation in skin injury model, and turned keratinocytes more vulnerable to ferroptosis induced by iron overload. The application of NMN markedly facilitated the NAD⁺/NADH system, increased the biosynthesis of GSH and inhibited the accumulation of lipid ROS in a GPX4-dependent manner. The administration of NMN or ferroptosis inhibitor might become effective approaches for treating UV irradiation-induced skin diseases.

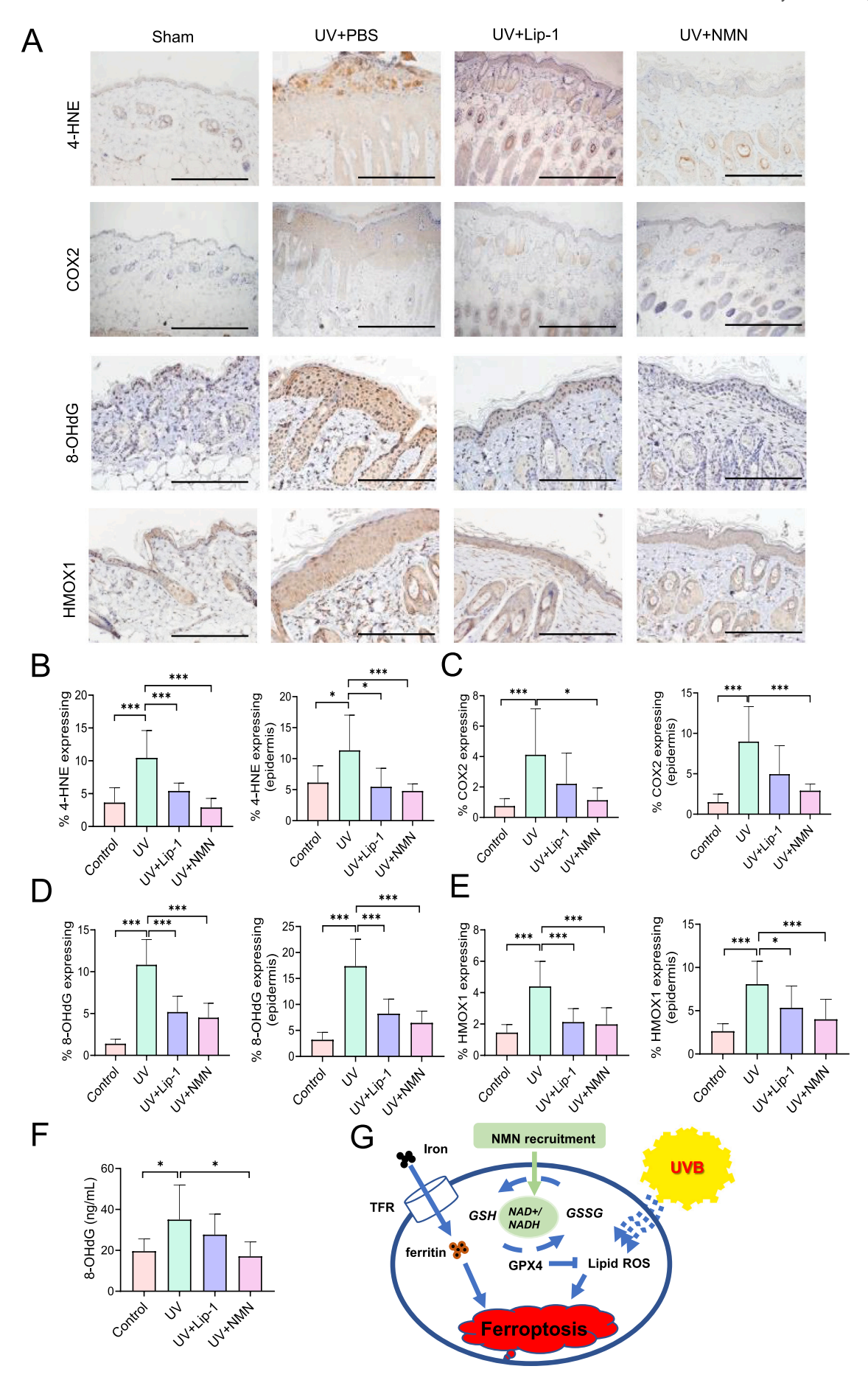


Fig. 8. NMN significantly decreased the accumulation of lipid peroxides. (A) Representative images of 4-HNE, COX2, 8-OHdG, and HMOX1 in dorsal skin of the Sham, UV, UV + Lip-1, and UV + NMN 4 groups at 7 d post-UV irradiation. (B-E) Quantification of the expression of 4-HNE, COX2, 8-OHdG, and HMOX1 (n=5 per group) in the experimental groups is shown. (F) The histograms show the concentration of 8-OHdG in serum of each group (n=5 per group) at 7 d post-UV irradiation. (G) Model illustrating the mechanism by which GPX4 suppresses ferroptosis in UVB induced skin injury and iron overload. Horizontal bars in all histograms denote the statistical significance between groups. P values were determined by one way-ANOVA. Scale bars: A, 10 μ m; n=3 per group. *p < 0.05; **p < 0.01; ***p < 0.001.

Credit authorship contribution statement

Zhuan Feng, YiFei Qin, Fei Huo, Zhe Jian, JieJie Geng, Yong Li and Jiao Wu conceived and designed the experiments. Zhuan Feng, YiFei Qin, Fei Huo, XiaoMin Li, JieJie Geng, Yong Li and Jiao Wu performed experiments. Zhuan Feng, YiFei Qin, Fei Huo analyzed the data and performed the statistical analyses. Zhuan Feng, Jiao Wu, JieJie Geng, Yong Li wrote the manuscript. All authors read and agreed to the final version of the manuscript.

Declaration of competing interest

The authors have no conflict of interest relevant to this study to declare.

Acknowledgments

This study was supported by the National Natural Science Foundation of China 82022059 (to J.W.), the Youth Science and Technology Nova Program of Shaanxi Province 2020KJXX-055 (to J.W.), and National Natural Science Foundation of China 31800756 (to J.J.G.).

Appendix A. Supplementary data

Supplementary data to this article can be found online at https://doi.org/10.1016/j.bbadis.2021.166287.

References

- D.L. Narayanan, J.L. Saladi Rn Fau Fox, J.L. Fox, Ultraviolet radiation and skin cancer, (1365-4632 (Electronic)).
- [2] J. D'Orazio, A. Jarrett S Fau Amaro-Ortiz, T. Amaro-Ortiz A Fau Scott, T. Scott, UV radiation and the skin, (1422–0067 (Print)).
- [3] A.P. Schuch, N.C. Moreno, N.J. Schuch, C.F.M. Menck, C.C.M. Garcia, Sunlight damage to cellular DNA: Focus on oxidatively generated lesions, (1873–4596 (Electronic)).
- [4] J.L. Ravanat, J. Douki T Fau Cadet, J. Cadet, Direct and indirect effects of UV radiation on DNA and its components, (1011–1344 (Print)).
- [5] S. Mukherjee, V. Date A Fau Patravale, H.C. Patravale V Fau Korting, A. Korting Hc Fau - Roeder, G. Roeder A Fau - Weindl, G. Weindl, Retinoids in the treatment of skin aging: an overview of clinical efficacy and safety, (1176–9092 (Print)).
- [6] T. Hakozaki, T. Date A Fau Yoshii, S. Yoshii T Fau Toyokuni, H. Toyokuni S Fau Yasui, H. Yasui H Fau Sakurai, H. Sakurai, Visualization and characterization of UVB-induced reactive oxygen species in a human skin equivalent model, (0340–3696 (Print)).
- [7] F.R. de Gruijl, Skin cancer and solar UV radiation, (0959-8049 (Print)).
- [8] G.M. Halliday, Inflammation, gene mutation and photoimmunosuppression in response to UVR-induced oxidative damage contributes to photocarcinogenesis, (0027–5107 (Print)).
- [9] M.J. Piao, S.J. Hyun Yj Fau Cho, H.K. Cho Sj Fau Kang, E.S. Kang Hk Fau Yoo, Y.S. Yoo Es Fau Koh, N.H. Koh Ys Fau Lee, M.H. Lee Nh Fau Ko, J.W. Ko Mh Fau Hyun, J.W. Hyun, An ethanol extract derived from Bonnemaisonia hamifera scavenges ultraviolet B (UVB) radiation-induced reactive oxygen species and attenuates UVB-induced cell damage in human keratinocytes, (1660–3397 (Electronic)).
- [10] T.S. Rafferty, C. Beckett Gj Fau Walker, Y.C. Walker C Fau Bisset, R.C. Bisset Yc Fau - McKenzie, R.C. McKenzie, Selenium protects primary human keratinocytes from apoptosis induced by exposure to ultraviolet radiation. (0307–6938 (Print)).
- [11] B.R. Stockwell, X.J. Jiang, W. Gu, Emerging mechanisms and disease relevance of ferroptosis, Trends Cell Biol. 30 (6) (2020) 478–490.
- [12] X.A.-O. Jiang, B.A.-O. Stockwell, M.A.-O. Conrad, Ferroptosis: mechanisms, biology and role in disease, (1471–0080 (Electronic)).
- [13] H. Tu, X.J. Tang Lj Fau Luo, K.L. Luo Xj Fau Ai, J. Ai Kl Fau Peng, J. Peng, Insights into the novel function of system Xc- in regulated cell death, (2284–0729 (Electronic)).
- [14] H.F. Yan, T. Zou, Q.Z. Tuo, S. Xu, H. Li, A.A.-O. Belaidi, P. Lei, Ferroptosis: mechanisms and links with diseases, (2059–3635 (Electronic)).

- [15] S. Imai, J. Yoshino, The importance of NAMPT/NAD/SIRT1 in the systemic regulation of metabolism and ageing, (1463–1326 (Electronic)).
- [16] J.R. Revollo, S.-i. Grimm Aa Fau Imai, S. Imai, The NAD biosynthesis pathway mediated by nicotinamide phosphoribosyltransferase regulates Sir2 activity in mammalian cells, (0021–9258 (Print)).
- [17] T. Wang, P. Zhang X Fau Bheda, J.R. Bheda P Fau Revollo, S.-i. Revollo Jr Fau Imai, C. Imai S Fau Wolberger, C. Wolberger, Structure of Nampt/PBEF/visfatin, a mammalian NAD+ biosynthetic enzyme, (1545–9993 (Print)).
- [18] C.C.S. Chini, J.D. Zeidler, S. Kashyap, G. Warner, E.N. Chini, Evolving concepts in NAD(+) metabolism, (1932–7420 (Electronic)).
- [19] A. Valavanidis, C. Vlachogianni T Fau Fiotakis, C. Fiotakis, 8-hydroxy-2'-deoxyguanosine (8-OHdG): a critical biomarker of oxidative stress and carcinogenesis, (1532–4095 (Electronic)).
- [20] A.A.-O. Ayala, M.F. Muñoz, S. Argüelles, Lipid peroxidation: production, metabolism, and signaling mechanisms of malondialdehyde and 4-hydroxy-2nonenal, (1942–0994 (Electronic)).
- [21] M.J. Bertoldo, D.R. Listijono, W.J. Ho, A.H. Riepsamen, D.M. Goss, D. Richani, X.L. Jin, S. Mahbub, J.M. Campbell, A. Habibalahi, W.N. Loh, N.A. Youngson, J. Maniam, A.S.A. Wong, K. Selesniemi, S. Bustamante, C. Li, Y. Zhao, M.B. Marinova, L.J. Kim, L. Lau, R.M. Wu, A.S. Mikolaizak, T. Araki, D.G. Le Couteur, N. Turner, M. J. Morris, K.A. Walters, E. Goldys, C. O'Neill, R.B. Gilchrist, D.A. Sinclair, H.A. Homer, L.E. Wu, NAD(+) repletion rescues female fertility during reproductive aging, (2211–1247 (Electronic)).
- [22] S. Xu, J. Min, F. Wang, Ferroptosis: an emerging player in immune cells, Sci. Bull. (2021), https://doi.org/10.1016/j.scib.2021.02.026.
- [23] Y. Xie, W. Hou, X. Song, Y. Yu, J. Huang, X. Sun, R. Kang, D. Tang, Ferroptosis: process and function, (1476–5403 (Electronic)).
- [24] B.R. Stockwell, J.P. Friedmann Angeli, H. Bayir, A.I. Bush, M. Conrad, S.J. Dixon, S. Fulda, S. Gascón, S.K. Hatzios, V.E. Kagan, K. Noel, X. Jiang, A. Linkermann, M. E. Murphy, M. Overholtzer, A. Oyagi, G.C. Pagnussat, J. Park, Q. Ran, C.S. Rosenfeld, K. Salnikow, D. Tang, F.M. Torti, S.V. Torti, S. Toyokuni, K.A. Woerpel, D.D. Zhang, Ferroptosis: a regulated cell death nexus linking metabolism, redox biology, and disease, (1097–4172 (Electronic)).
- [25] A.A.-O. Linkermann, R. Skouta, N. Himmerkus, S.R. Mulay, C. Dewitz, F. De Zen, A. Prokai, G. Zuchtriegel, F. Krombach, P.S. Welz, R. Weinlich, T. Vanden Berghe, P. Vandenabeele, M. Pasparakis, M. Bleich, J.M. Weinberg, C.A. Reichel, J.H. Bräsen, U. Kunzendorf, H.J. Anders, B.R. Stockwell, D.R. Green, S. Krautwald, Synchronized renal tubular cell death involves ferroptosis, (1091–6490 (Electronic)).
- [26] Q.Z. Tuo, P. Lei, K.A. Jackman, X.L. Li, H. Xiong, X.L. Li, Z.Y. Liuyang, L. Roisman, S.T. Zhang, S. Ayton, Q. Wang, P.J. Crouch, K. Ganio, X.C. Wang, L. Pei, P.A. Adlard, Y.M. Lu, R. Cappai, J.Z. Wang, R. Liu, A.I. Bush, Tau-mediated iron export prevents ferroptotic damage after ischemic stroke, (1476–5578 (Electronic)).
- [27] X.A.-O. Fang, H.A.-O. Wang, D. Han, E. Xie, X. Yang, J. Wei, S. Gu, F. Gao, N. Zhu, X. Yin, Q. Cheng, P. Zhang, W. Dai, J. Chen, F. Yang, H.T. Yang, A.A.-O. Linkermann, W.A.-O. Gu, J.A.-O. Min, F.A.-O. Wang, Ferroptosis as a target for protection against cardiomyopathy, (1091–6490 (Electronic)).
- [28] M.J. Smith, M. Fowler, R.J. Naftalin, R.C.M. Siow, UVA irradiation increases ferrous iron release from human skin fibroblast and endothelial cell ferritin: consequences for cell senescence and aging, (1873–4596 (Electronic)).
- [29] I. Ingold, C. Berndt, S. Schmitt, S. Doll, G. Poschmann, K. Buday, A. Roveri, X. Peng, F. Porto Freitas, T. Seibt, L. Mehr, M. Aichler, A. Walch, D. Lamp, M. Jastroch, S. Miyamoto, W. Wurst, F. Ursini, E.S.J. Arnér, N. Fradejas-Villar, U. Schweizer, H. Zischka, J.P. Friedmann Angeli, M. Conrad, Selenium utilization by GPX4 is required to prevent hydroperoxide-induced ferroptosis, (1097–4172 (Electronic)).
- [30] K. Shimada, M. Hayano, N.C. Pagano, B.R. Stockwell, Cell-line selectivity improves the predictive power of pharmacogenomic analyses and helps identify NADPH as biomarker for ferroptosis sensitivity, (2451–9448 (Electronic)).
- [31] C.C. Ding, J.A.-O. Rose, T. Sun, J. Wu, P.H. Chen, C.A.-O. Lin, W.A.-O. Yang, K.Y. Chen, H. Lee, E. Xu, S. Tian, J. Akinwuntan, J. Zhao, Z. Guan, P.A.-O. Zhou, J.A.-O. X. Chi, MESH1 is a cytosolic NADPH phosphatase that regulates ferroptosis, (2522–5812 (Electronic)).
- [32] N. Pollak, M. Dölle C Fau Ziegler, M. Ziegler, The power to reduce: pyridine nucleotides-small molecules with a multitude of functions, (1470–8728 (Electronic)).
- [33] L.R. Stein, S. Imai, Specific ablation of Nampt in adult neural stem cells recapitulates their functional defects during aging, (1460–2075 (Electronic)).
- [34] W. Xiao, R.S. Wang, D.E. Handy, J. Loscalzo, NAD(H) and NADP(H) redox couples and cellular energy metabolism, (1557–7716 (Electronic)).
- [35] S. Oka, J. Hsu Cp Fau Sadoshima, J. Sadoshima, Regulation of cell survival and death by pyridine nucleotides, (1524–4571 (Electronic)).
- [36] J. Yoshino, M.J. Mills Kf Fau Yoon, S.-i. Yoon Mj Fau Imai, S. Imai, Nicotinamide mononucleotide, a key NAD(+) intermediate, treats the pathophysiology of dietand age-induced diabetes in mice, (1932–7420 (Electronic)).
- [37] C.B. Peek, K.M. Affinati Ah Fau Ramsey, H.-Y. Ramsey Km Fau Kuo, W. Kuo Hy Fau Yu, L.A. Yu W Fau Sena, O. Sena La Fau Ilkayeva, B. Ilkayeva O Fau -

- Marcheva, Y. Marcheva B Fau Kobayashi, C. Kobayashi Y Fau Omura, D.C. Omura C Fau Levine, D.J. Levine Dc Fau Bacsik, D. Bacsik Dj Fau Gius, C.B. Gius D Fau Newgard, E. Newgard Cb Fau Goetzman, N.S. Goetzman E Fau Chandel, J.M. Chandel Ns Fau Denu, M. Denu Jm Fau Mrksich, J. Mrksich M Fau Bass, J. Bass, Circadian clock NAD+ cycle drives mitochondrial oxidative metabolism in mice, (1095–9203 (Electronic)).
- [38] K.L. Stromsdorfer, S. Yamaguchi, M.J. Yoon, A.C. Moseley, M.P. Franczyk, S.C. Kelly, N. Qi, S. Imai, J. Yoshino, NAMPT-mediated NAD(+) biosynthesis in adipocytes regulates adipose tissue function and multi-organ insulin sensitivity in mice, (2211–1247 (Electronic)).
- [39] A.S. Martin, D.M. Abraham, K.A. Hershberger, D.P. Bhatt, L. Mao, H. Cui, J. Liu, X. Liu, M.J. Muehlbauer, P.A. Grimsrud, J.W. Locasale, R.M. Payne, M.D. Hirschey, Nicotinamide mononucleotide requires SIRT3 to improve cardiac function and bioenergetics in a Friedreich's ataxia cardiomyopathy model. LID 93885 [pii] LID https://doi.org/10.1172/jci.insight.93885 [doi] LID e93885, (2379–3708 (Electronic)).
- [40] A.P. Gomes, N.L. Price, A.J. Ling, J.J. Moslehi, M.K. Montgomery, L. Rajman, J.P. White, J.S. Teodoro, C.D. Wrann, B.P. Hubbard, E.M. Mercken, C.M. Palmeira, R. de Cabo, A.P. Rolo, N. Turner, E.L. Bell, D.A. Sinclair, Declining NAD(+) induces a

- pseudohypoxic state disrupting nuclear-mitochondrial communication during aging, (1097–4172 (Electronic)).
- [41] Y. Guan, S.R. Wang, X.Z. Huang, Q.H. Xie, Y.Y. Xu, D. Shang, C.M. Hao, Nicotinamide mononucleotide, an NAD(+) precursor, rescues age-associated susceptibility to AKI in a sirtuin 1-dependent manner, (1533–3450 (Electronic)).
- [42] J.B. Lin, S. Kubota, N. Ban, M. Yoshida, A. Santeford, A. Sene, R. Nakamura, N. Zapata, M. Kubota, K. Tsubota, J. Yoshino, S.I. Imai, R.S. Apte, NAMPT-mediated NAD(+) biosynthesis is essential for vision in mice, (2211–1247 (Electronic)).
- [43] S. Tarantini, M.N. Valcarcel-Ares, P. Toth, A. Yabluchanskiy, Z. Tucsek, T. Kiss, P. Hertelendy, M. Kinter, P. Ballabh, Z. Süle, E. Farkas, J.A. Baur, D.A. Sinclair, A. Csiszar, Z. Ungvari, Nicotinamide mononucleotide (NMN) supplementation rescues cerebromicrovascular endothelial function and neurovascular coupling responses and improves cognitive function in aged mice, (2213–2317 (Electronic)).
- [44] L. Hosseini, M.S. Vafaee, R.A.-O. Badalzadeh, melatonin and nicotinamide mononucleotide attenuate myocardial ischemia/reperfusion injury via modulation of mitochondrial function and hemodynamic parameters in aged rats, (1940–4034 (Electronic)).
- [45] N. Xie, L. Zhang, W. Gao, C.A.-O. Huang, P.E. Huber, X. Zhou, C. Li, G. Shen, B.A.-O. Zou, NAD(+) metabolism: pathophysiologic mechanisms and therapeutic potential, (2059-3635 (Electronic)).